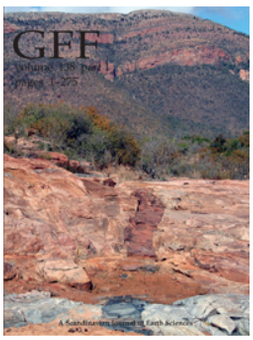

GFF

ISSN: 1103-5897 (Print) 2000-0863 (Online) Journal homepage: http://www.tandfonline.com/loi/sgff20

The ca. 1.8 Ga mantle plume related magmatism of the central part of the Ukrainian shield

Leonid Shumlyanskyy, Oleksandr Mitrokhin, Kjell Billström, Richard Ernst, Eugenia Vishnevska, Stepan Tsymbal, Michel Cuney & Alvar Soesoo

To cite this article: Leonid Shumlyanskyy, Oleksandr Mitrokhin, Kjell Billström, Richard Ernst, Eugenia Vishnevska, Stepan Tsymbal, Michel Cuney & Alvar Soesoo (2016) The ca. 1.8 Ga mantle plume related magmatism of the central part of the Ukrainian shield, GFF, 138:1, 86-101, DOI: 10.1080/11035897.2015.1067253

To link to this article: http://dx.doi.org/10.1080/11035897.2015.1067253

Published online: 16 Dec 2015.

GFF, 2016
Vol. 138, No. 1, 86–101, http://dx.doi.org/10.1080/1331677X.2015.1067253

Article

The ca. 1.8 Ga mantle plume related magmatism of the central part of the Ukrainian shield

LEONID SHUMLYANSKYY[1], OLEKSANDR MITROKHIN[2], KJELL BILLSTRÖM[3], RICHARD ERNST[4,5], EUGENIA VISHNEVSKA[2], STEPAN TSYMBAL[1], MICHEL CUNEY[6] and ALVAR SOESOO[7]

Shumlyanskyy, L., Mitrokhin, O., Billström, K., Ernst, R., Vishnevska, E., Tsymbal, S., Cuney, M., & Soesoo, A., 2015: The ca. 1.8 Ga mantle plume related magmatism of the central part of the Ukrainian shield. *GFF*, Vol. 138, No. 1, pp. 86–101. © Geologiska Föreningen. doi: http://dx.doi.org/10.1080/11035897.2015.1067253.

Abstract: Palaeoproterozoic (ca. 1.8 Ga) mafic and ultramafic dykes are widely distributed within the whole Sarmatian segment of the East-European craton. This paper focuses on new geochronological, geochemical and isotope data obtained for mafic and ultramafic dykes of the Ingul terrain. Geochronological data available for these dykes indicate ages around 1800 Ma. We provide a new U–Pb zircon age of 1810 ± 15 Ma obtained for a dolerite dyke in the Kirovograd area. Geochemical and petrographical data allow identification of three groups of dykes: (1) kimberlites, (2) high-Mg# subalkaline rocks (picrite, camptonite, subalkaline dolerite etc.) and (3) tholeiite dolerite. Rocks of these groups were probably derived from different sources. εNd_{1800} values of studied rocks vary from 0.7 to 2.8. The highest values were obtained for mantle xenoliths and their kimberlite host (εNd_{1800} = 2.5–2.8). Rb–Sr data yield a regression age of 1729 ± 20 Ma with an initial $^{87}Sr/^{86}Sr = 0.70366 \pm 41$ (MSWD = 10.8). The whole-rock lead isotope data scatter, but data for sub-groups of samples can tentatively be fitted to parallel 1.8 Ga isochrons. The geochemical data indicate rocks to have formed by partial melting and the degree of melting is thought to be a function of formation depth, the latter ranging from sub-lithospheric to lower-crustal levels; we assume that melting was caused by a mantle plume. Dyking in the Ingul terrain was closely associated in time and space with metasomatic albitites that host numerous economic U deposits.

Keywords: palaeoproterozoic; U–Pb geochronology; ukrainian shield; mafic dykes; Sr–Nd–Pb isotope composition; mantle sources

[1]*Institute of Geochemistry, Mineralogy and Ore Formation of the National Academy of Sciences of Ukraine, Palladina Ave. 34, 03680 Kyiv, Ukraine; lshumlyanskyy@yahoo.com, tsymbal@igmof.gov.ua;*

[2]*Geological Department, Kyiv Taras Shevchenko National University, Vasylkivska st., 90, 03022 Kyiv, Ukraine; Mitrokhin.A.V@yandex.ua, genyvishnevskia@mail.ru;*

[3]*Department for Geological Sciences, Swedish Museum of Natural History, P.O. Box 50 007, SE-10405 Stockholm, Sweden; kjell.billstrom@nrm.se;*

[4]*Department of Earth Sciences, Carleton University, Ottawa, Ontario K1S 5B6, Canada; Richard.Ernst@ErnstGeosciences.com;*

[5]*Faculty of Geology and Geography, Tomsk State University, 36 Lenin Ave, Tomsk 634050, Russia;*

[6]*GeoRessources UMR 7359, Université de Lorraine-CNRS-CREGU, Vandœuvre-lès-Nancy, France; michel.cuney@univ-lorraine.fr;*

[7]*Institute of Geology, Tallinn University of Technology, Building IVC, Ehitajate tee 5, Tallinn 19086, Estonia; alvar.soesoo@gmail.com*

Manuscript received 05 February 2015; accepted 21 June 2015.

Introduction

Continental flood basalt (CFB) provinces represent a particular case of large igneous provinces (LIPs) that occur as "anomalous magmatic events … during which large volumes of mafic and generally subordinate silicic and ultramafic magmas were generated and emplaced by processes distinct from those observable at modern plate boundaries, and predicted by plate-tectonic

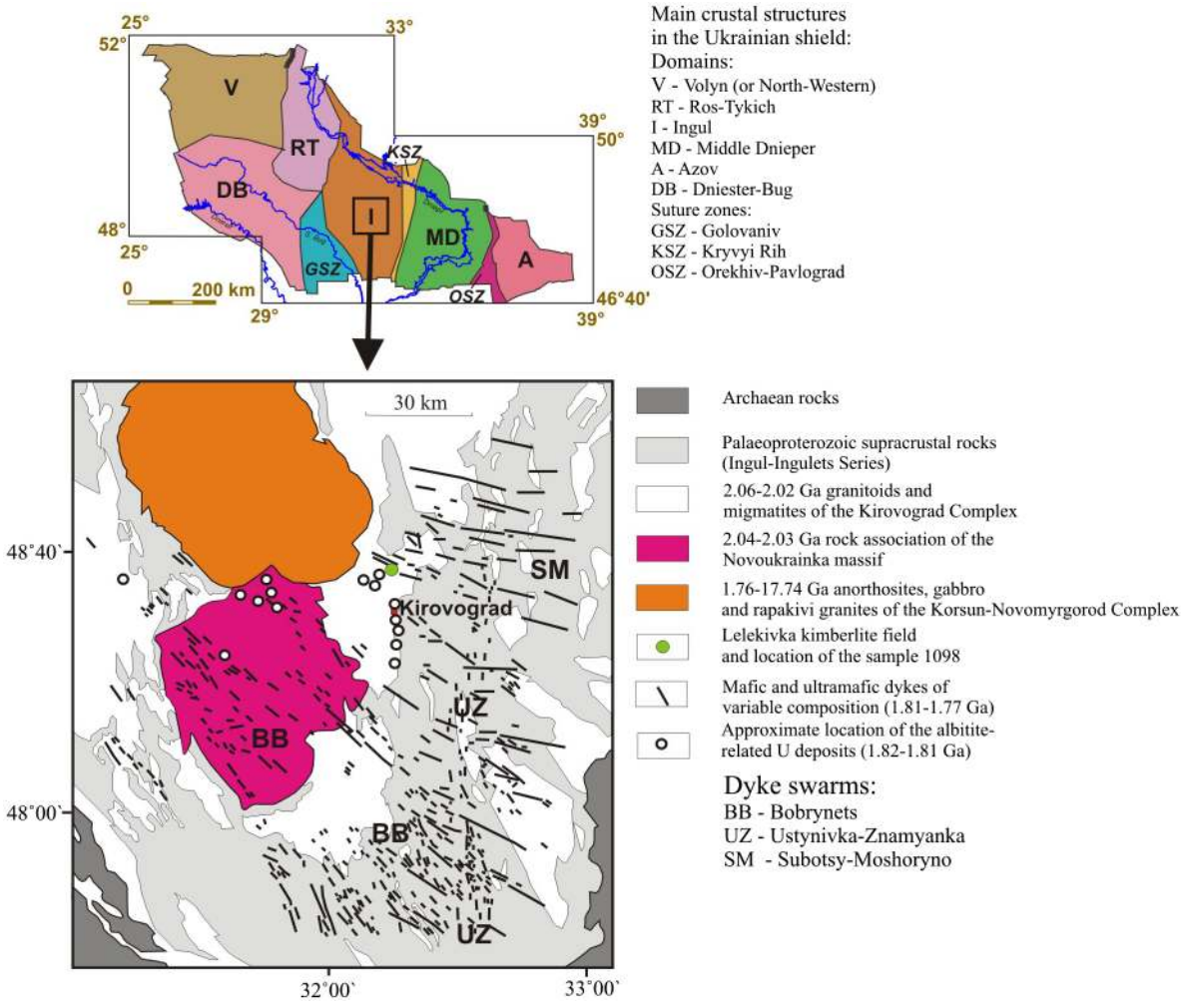

Fig. 1. Schematic geological map of the Ukrainian shield (Claesson et al., 2015) and the central part of the Ingul terrain, modified after Bogdanova et al. (2013); location of the U deposits according to Cuney et al. (2012).

theory" (Bryan & Ernst 2008, p. 175; Ernst 2014). A typical CFB province occurs as a thick pile of basalt-family effusive rocks, distributed over a large area, that got erupted during a relatively short (a few myr) interval of time. Formation of CFB provinces is usually related to the emplacement of a mantle plume that provides both heat required for extensive melting of the mantle and fusible enriched material that melts as plume ascends. Besides basaltic sequences, CFB provinces also include feeders (dykes) and intermediate chambers (layered intrusions). In terms of geochemical composition, rocks of gabbroic (basaltic) composition are predominant, although ultramafic rocks (picrites, meimechites, kimberlites) may also be common, as well as felsic rocks (rhyolites). Thick basaltic sequences are common for relatively young CFBs, while in older (Precambrian) provinces these are often eroded exposing the "roots" of the provinces represented by dykes, sills and layered intrusions.

The Ukrainian shield and its slopes host two Precambrian LIPs – the Vendian (c. 570 Ma) Volyn CFB province in which a c. 400 m thick pile of basaltic rocks is still preserved (Shumlyanskyy et al. 2007; Shumlyanskyy 2012), and the Palaeoproterozoic (c. 1800–1780 Ma) Prutivka-Novogol province that embraces numerous dykes and layered intrusions widely distributed throughout the Ukrainian shield and the Voronezh crystalline massif. Palaeoproterozoic dykes of the North-Western region of the Ukrainian shield have previously been extensively studied and dated (Shumlyanskyy 2008; Elming et al. 2010; Shumlyanskyy et al. 2012; Bogdanova et al. 2013). However, the dykes of the central part of the shield (Ingul Domain) have been less thoroughly investigated (Nikolsky 1974; Krutikhovskaya et al. 1976; Hrechishnikov et al. 1980). More recently, also the kimberlites of the Kirovograd area and their mantle xenoliths have been investigated (Tsymbal et al. 1999; Bogdanova et al. 2013).

In this paper we present new whole-rock geochemical and isotope (Sr, Nd and Pb isotopes) data, and geochronological (U–Pb zircon) results obtained for various dykes from the Ingul Domain of the Ukrainian shield. We discuss the origin of these rocks, their relation to coeval dykes found in the North-Western region of the Ukrainian shield, and possible links to regional metasomatic alteration and associated U deposits.

Geological setting

The studied area is located in the central part of the Ukrainian shield, within the mainly Palaeoproterozoic Ingul Domain (Fig. 1). This domain is separated from the neighbouring Ros-Tikych and Dniester-Bug Domains by the Golovanivsk shear zone, and from the Middle Dnieper Domain by the Ingulets-Kryvy Rih shear zone. The oldest supracrustal rocks within the Ingul Domain belong to the Ingul-Ingulets Series that embraces gneisses, schists, amphibolites, quartzites, marbles and calc-silica rocks metamorphosed in epidote-amphibolite to granulite facies (Usenko et al. 1982). Biotite and garnet-biotite granites together with aplite and pegmatite granites of the Kirovograd Complex form large intrusive massifs, whereas migmatites developed after the supracrustals of the Ingul-Ingulets Series. The ages obtained for the Kirovograd Complex granites vary from c. 2060 to 2020 Ma (Stepanyuk et al. 2012; Shestopalova et al., 2013), while the Novoukrainka Complex, comprising the large Novoukrainka gabbro-monzonite-granite massif and several smaller massifs, was formed at c. 2040 Ma (Stepanyuk et al. 2005; Cuney et al. 2008).

The large Korsun–Novomyrgorod anorthosite–mangerite–rapakivi granite Plutonic Complex (KNPC) occupies the central part of the domain and cuts all of the above-described rock complexes. The age of the KNPC is defined as 1.76–1.74 Ga (Scherbak et al. 2008). Numerous metasomatic (albitite) uranium deposits are known near the southern contact of the KNPC within rocks of the Novoukrainka and Kirovograd Complexes (Cuney et al. 2012). Taking into account their absence (and lack of metasomatic mineralization) within the KNPC, it is inferred that they formed before c. 1760 Ma. The age of these deposits is poorly constrained at c. 1810 Ma (Scherbak et al. 2008).

Numerous mafic dykes occur in the Ingul Domain and vary widely in composition, including e.g., dolerite, picrite, camptonite and kimberlite. Dykes are up to 10–20 m wide, steep to subvertical in dip, and some of them can be traced along strike for tens of km. Dykes are especially abundant in the vicinity of the KNPC where they form numerous swarms arranged in a fan-like pattern (Fig. 1). In the north-eastern part dykes are west–east trending, while towards the south their direction gradually changes to northwest-southeast. According to Bogdanova et al. (2013) dykes converge to a common point west of the KNPC. It is interesting to note that the locus of this fan-like pattern approximately coincides with the area of the most developed Na-metasomatism. Some of the dykes were subjected to Na-metasomatism whereas others cut metasomitized rocks and contain albitite xenoliths; these observations may indicate the presence of several generations of dykes (Tsymbal 2013; Zankevych et al. 2014). Noting that the dykes cut Palaeoproterozoic granitoids of the Kirovograd and Novoukrainka Complexes, as well as rocks of the Ingul-Ingulets Series; and yet absent in the KNPC and neither present in the adjacent Ros-Tikych and Dniester-Bug Domains (Scherbakov 2005) constrain the age of dykes between c. 2.0 and 1.75 Ga.

Methods

Zircons were separated at the Institute of Geochemistry, Mineralogy and Ore Formation using standard methods. The final selection of the zircon grains for U–Pb dating was done by hand-picking under a binocular microscope. Zircon grains were mounted in a resin puck and polished to half of their thickness. Zircons were analyzed for U, Th and Pb isotopes by the LA-ICP-MS technique at the Museum für Mineralogie und Geologie (GeoPlasma Lab, Senckenberg Naturhistorische Sammlungen Dresden), using a Thermo-Scientific Element 2 XR sector field ICP-MS coupled to a New Wave UP-193 Excimer Laser System. Each analysis consisted of 15 s background acquisition followed by 30 s data acquisition, using a laser spot-size of 35 µm. Raw data were corrected for background signal, common Pb, laser-induced elemental fractionation, instrumental mass discrimination and time-dependant elemental fractionation of Pb/Th and Pb/U. Reported uncertainties were propagated by quadratic addition of the external reproducibility obtained from the standard zircon GJ-1 (~0.6% and 0.5–1% for $^{207}Pb/^{206}Pb$ and $^{206}Pb/^{238}U$, respectively). For further details on the analytical protocol and data processing, see Gerdes and Zeh (2006). Th/U ratios, together with U and Pb contents, were determined from LA-ICP-MS data and calculated relative to the GJ-1 zircon standard; numbers are accurate to within approximately 10%.

Whole-rock samples were analysed for Nd, Sr and Pb isotopes at the Swedish Museum of Natural History, Stockholm, Sweden. Nd and Sm concentrations were determined by isotope dilution using a mixed ^{150}Nd–^{147}Sm spike. The Nd and Sr isotopic compositions were measured on a Thermo-Scientific TRITON instrument in static mode. Nd runs were corrected for fractionation to $^{146}Nd/^{144}Nd = 0.7219$, and estimated errors for $^{147}Sm/^{144}Nd$ are <0.5%. The Sr isotopic composition was measured on unspiked samples and data were normalized to $^{86}Sr/^{88}Sr = 0.1194$. Sr and Rb concentrations were obtained by the ICP-MS method. The lead isotope measurements were performed with a Multi-Collector Inductively Coupled Plasma Mass Spectrometer (MC-ICP-MS) of the type Micromass Isoprobe. The mass bias correction was made by adding thallium to the sample. Details are described in e.g., De Ignacio et al. (2006). The total error for reported Pb isotope compositions of unknowns is estimated to be ±0.1% or lower.

Whole rock analyses (major and trace elements) were produced at the CRPG-CNRS laboratory (Nancy; France) and at the Institute of Geology, Tallinn University of Technology. At the CRPG-CNRS laboratory analyses were obtained by ICP-OES and ICP-MS spectrometry ($LiBO_2$ fusion). Sample preparation, analytical conditions and limits of detection are detailed in Carignan et al. (2001). At the Tallinn University of Technology ICP-MS analyses were performed using a Thermo Scientific quadrupole X-Series 2 instrument. Whole-rock trace elements were determined from solutions which were prepared following the nitric, hydrofluoric, hydrochloric and boric acids digestion of a 0.250 g pulverized sample in an Anton Paar MW3000 microwave oven. The whole-rock major elements were analysed by XRF from glass disks, which were prepared using a Li-borate mix with pulverized sample (Claisse instrument). The S4 Pioneer Spectrometer (Bruker AXS GmbH, Germany), utilizing an X-ray tube with a rhodium anode, operated with a power of 3 kW.

Petrography

Basically, there are three main mafic and ultramafic dyke types in the Ingul Domain. The first group includes kimberlites, the second group – various high-Mg# subalkaline rocks (picrite,

camptonite, subalkaline dolerite etc.), and the third group embraces tholeiitic dolerites. Dykes of the first and second groups were found in close association in the north-eastern part of the studied area, nearby the city of Kirovograd, whereas the third group, tholeiitic dolerites, is widely distributed elsewhere in the area. According to Tsymbal et al. (1999), kimberlites of the Kirovograd area occur as fine-medium-grained porphyric rocks that contain numerous fragments (xenoliths) of mantle and lower-crustal rocks. Main rock-forming minerals are olivine (50–80%) and phlogopite (10–50%). Less abundant are magnetite, titanomagnetite, diopside, amphibole (tremolite or richterite), carbonates, chromite, apatite, perovskite, sulphides and secondary minerals like serpentine. The nature of carbonates is not always clear; in most cases these minerals are secondary, but primary magmatic carbonates may be also present (as interstitial calcite that is associated with diopside). A calcite-bearing variety of mica kimberlite enriched with apatite (up to 5%) was also noted. Olivine occurs as the earliest mineral in kimberlites where it forms rather large (up to 1–2 mm) porphyritic crystals set in a fine-grained magnetite-carbonate-phlogopite groundmass. Finer olivine crystals are also present. Due to the large degree of secondary alteration, the chemical composition of olivine remains unknown. Phlogopite is the second most important mineral in the rock and occurs as large (2–3 mm) laths that contain numerous inclusions of olivine and opaque minerals. In addition, phlogopite forms abundant microliths that enwind crystals of olivine and fragments of mantle and lower-crustal rocks. Diopside is present in the groundmass where it is extremely unevenly distributed. Its abundance may reach 15–20% to 40–50%, but usually it makes up less than a few %. There are two generations of diopside: the first generation occurs together with olivine and phlogopite as euhedral to anhedral groundmass grains, while the second generation occurs in association with calcite in carbonate-rich clusters. One kimberlite sample from the Levekivka kimberlite field (Fig. 1) was chosen for analysis.

Xenoliths in kimberlites vary in size from discrete grains to large (10–15 cm) fragments with irregular to rounded shape and rough to smooth surface. There are no signs of thermal or metasomatic influence of the host kimberlite on the xenoliths. Tsymbal and Kryvdik (1999) distinguished five main petrographical types of xenoliths in the Kirovograd kimberlites: (1) predominantly olivine rocks – dunites and peridotites; (2) Cr-spinel-bearing peridotites – harzburgites and lherzolites; (3) garnet-bearing eclogitic rocks; (4) high-Al and high-Fe ultrabasites (orthopyroxenites?); (5) glimmerites. We studied three samples of peridotites. These rocks are usually heavily altered with primary minerals represented by Cr-spinel and, rarely, by clinopyroxene. Olivine-bearing peridotites prevail with olivine having been completely replaced by serpentine. The amount of orthopyroxene may reach 20–30%, whereas clinopyroxene occurs in lower amounts (5–10%). Orthopyroxene is replaced by serpentine, talc and anthophyllite (up to 4% of Al_2O_3), whereas clinopyroxene is usually replaced by carbonate and talc.

Subalkaline dykes prevail within the Ustynivka-Znamyanka dyke swarm (Fig. 1), which is located in the central part of the Ingul Domain and was traced for about 100 km, and has a width of c. 30–35 km. The main rock type here is gabbro that consists of various amounts of olivine, Ti-augite, kaersutite, Ti-biotite, plagioclase, potassic feldspar, ilmenite and magnetite. Olivine usually forms large grains or segregations of grains; its concentration may vary along a vertical section of the dyke with some accumulation in the lower parts of inclined dykes. Olivine is usually replaced by serpentine and talc. Ti-augite occurs as fine crystals or glomerophyric grains which are up to 2–6 mm long. Kaersutite forms rather large (1–2 mm) elongated prismatic crystals that contain inclusions of olivine, Ti-augite and apatite. Some of the kaersutite crystals are rimmed by greenish-blue alkaline hornblende. Biotite associates with amphibole and opaque minerals.

In addition, dykes composed of fresh olivine dolerite prevail in the Bobrynets dyke swarm (Fig. 1). Dolerites have generally a fully crystalline ophitic texture, while a poikilo-ophitic texture was found in few specimens. Most of the samples contain a small (<5%) amount of plagioclase microphenocrysts. Main rock-forming minerals are plagioclase and clinopyroxene whereas olivine, ilmenite, titanomagnetite, pyrrhotite, apatite, quartz, K-feldspar and biotite are minor or accessory phases. The groundmass plagioclase, occasionally reaching 65–70%, occurs as 0.6–1.0 mm long laths composed of andesine-labradorite $An_{41–67}$, whereas tabular porphyric crystals are 2–3 mm long and made of bytownite $An_{70–83}$ in core portions and labradorite $An_{51–62}$ in outer rims. Clinopyroxene is a major mafic groundmass mineral. It fills the space between plagioclase laths and varies in composition from pigeonite $Wo_{8–15}En_{53–67}$ to subcalcic augite $Wo_{16–21}En_{48–59}$ and augite $Wo_{28–38}En_{37–54}$. The olivine amount does usually not exceed 10%. It occurs as subhedral, isometric grains that vary in size from 0.1 to 0.5 mm and in composition from $Fo_{70–76}$ in cores to $Fo_{40–47}$ in rims.

Geochemistry

The three groups of mafic and ultramafic dykes recognized in the Ingul Domain can also be considered from a chemical point of view (Fig. 2). Neither of the mentioned rocks contain any significant amount of cumulative phases, so their composition closely corresponds to that of their parental melts, when effects of the secondary alteration are taken into account.

Following the work of Tsymbal et al. (1999) and Bogdanova et al. (2013) the first group of high-Mg (Mg# = 74–87) rocks which vary widely in composition (SiO_2 = 33.5–51.0%, TiO_2 = 0.9–4.6%, Al_2O_3 = 1.5–10.4%, CaO = 3.1–12.4% etc.), is described here as a kimberlite group dominated by micaceous kimberlites or olivine lamproites (Tsymbal et al. 1999). These rocks are characterized by very high concentrations of both incompatible and compatible trace elements (Fig. 2). Investigations of the chemical composition of the Kirovograd kimberlites are complicated by the high degree of alteration that is displayed mainly in an increased concentration of SiO_2, H_2O and CO_2, and decreased abundances of MgO and K_2O. Large variations in the phenocryst-to-groundmass ratio and the presence of a large amount of xenoliths of variable composition add further complexity. Hence, pronounced evolutionary trends seen on variation diagrams (Fig. 2) may not be related to the real compositional variation of the initial melts.

The second group embraces a large variety of high-Ti mafic to ultramafic subalkaline rocks that range in Mg# from 44 to 70, SiO_2 – from 37.5% to 43.0%, TiO_2 – from 2.7% to 7.8%, Al_2O_3 – from 6.2% to 13.6% and CaO – from 3.7% to 10.6% etc. The chemical compositions of these rocks presented by Bogdanova et al. (2013) demonstrate a regular variation with Mg#: concentrations of TiO_2, CaO, Na_2O, Sr, Nb, Cu and V gradually increase as Mg# decreases, while SiO_2, Ni and Cr display an opposite tendency (Fig. 2). A pronounced geochemical feature

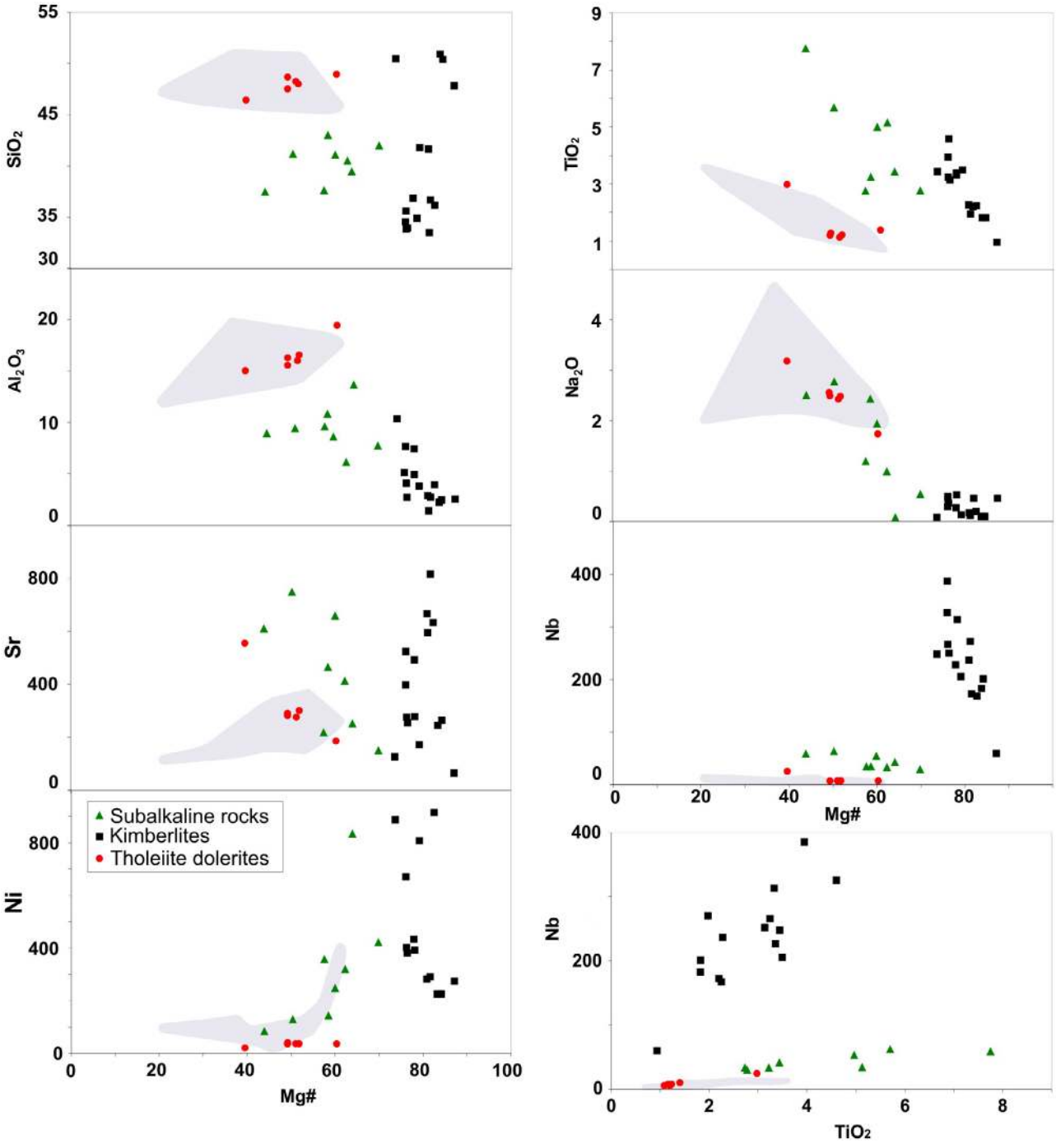

Fig. 2. Chemical variation diagrams for mafic and ultramafic dykes of the Ingul terrain. Shaded area indicates compositions of contemporaneous tholeiite dykes of the North-Western region of the Ukrainian shield (chemical analyses from Tsymbal et al., 1999; Shumlyanskyy, 2008; Bogdanova et al., 2013, and new analyses by the authors).

of these rocks is a high to very high concentration of TiO_2 whereas the Nb concentration remains at a relatively low level (30–60 ppm compared to 5–6 ppm in the tholeiite group and 60–385 ppm in kimberlite).

Finally, the third group is represented by typical tholeiite dolerite dykes (Table 1). These rocks are quite homogeneous in their composition (with the exception of sample 3425/105.0 that is characterized by a high degree of secondary alteration) and their Mg# range from 40 to 60. In contrast to the kimberlites and the subalkaline high-Ti rocks, respectively, the tholeiite dykes do not demonstrate any significant variations in abundances of major oxides (Fig. 2).

The evolutionary trends defined for all three groups of rocks do not follow each other and demonstrate independent behaviour. However, there are some general trends that link all three groups of dykes. For instance, the concentration of Al_2O_3 and Na_2O gradually rises from kimberlites to tholeiite dolerites indicating the increased role of plagioclase in the latter.

Table 1. Chemical compositions of tholeiite dykes.

Sample	3417/45.3	3419/212.5	3420/205.8	3424/287.4	3425/105.0
SiO_2	48.04	48.64	48.22	47.61	48.91
TiO_2	1.18	1.21	1.12	1.18	1.40
Al_2O_3	16.60	16.33	16.02	15.66	19.41
Fe_2O_3	12.36	13.59	14.33	15.26	12.14
MnO	0.31	0.19	0.19	0.19	0.23
MgO	6.31	6.29	7.17	7.06	8.77
CaO	11.05	9.80	9.69	9.23	2.80
Na_2O	2.48	2.56	2.41	2.46	1.76
K_2O	0.51	0.52	0.57	0.55	3.44
P_2O_5	0.17	0.20	0.18	0.19	0.18
LOI	0.02	1.22	0.66	1.32	6.30
Total	99.20	100.55	100.57	100.70	99.24
Li	11	–	–	–	91
Be	0.8	0.5	0.4	0.5	1.0
Sc	33	37	34	35	11
V	189	199	183	192	204
Cr	101	114	105	110	98
Co	61	53	50	51	54
Ni	38	39	38	38	3
Cu	28	29	27	27	30
Zn	11	121	101	106	105
Ga	16	20	19	19	19
Ge	–	2.0	1.9	2.3	–
Rb	12.3	12.1	18.0	23.1	182.4
Sr	300.5	287.1	276.7	279.6	186.6
Y	25.1	25.0	20.7	22.0	17.7
Zr	–	85	76	83	–
Nb	5.7	5.2	4.9	5.1	6.5
Mo	1.0	0.9	0.8	0.9	0.7
Sn	–	1.0	3.1	1.1	–
Cs	0.5	0.8	1.3	2.1	2.5
Ba	229	200	184	183	506
La	11.25	9.74	8.65	8.88	7.88
Ce	24.08	22.72	20.18	21.03	18.81
Pr	3.35	3.09	2.73	2.90	2.65
Nd	15.06	13.97	12.49	13.21	12.07
Sm	3.78	3.56	3.12	3.27	3.07
Eu	1.36	1.27	1.13	1.16	1.27
Gd	4.36	3.77	3.20	3.44	3.55
Tb	0.70	0.64	0.56	0.58	0.58
Dy	4.58	4.00	3.45	3.64	3.70
Ho	0.95	0.85	0.71	0.76	0.77
Er	2.75	2.37	2.00	2.13	2.19
Tm	0.40	0.35	0.31	0.33	0.32
Yb	2.57	2.35	2.05	2.18	2.07
Lu	0.39	0.38	0.33	0.35	0.31
Hf	–	2.3	2.0	2.2	–
Ta	–	0.5	0.7	0.5	–
W	–	0.5	0.4	0.6	–
Pb	1.8	1.8	1.7	1.7	2.3
Th	0.9	0.9	0.7	0.9	0.8
U	35.3	0.3	0.2	0.3	0.3

Geochemical differences between the three groups of dykes are easily seen on REE and trace elements spidergrams (Fig. 3). Kimberlites demonstrate the most fractionated REE patterns [(La/Yb)n = 75–260], high-Ti subalkaline rocks are less fractionated [(La/Yb)n = 9–25], while the REE pattern in the tholeiites is almost flat [(La/Yb)n = 2.6–3.0]. Both kimberlites and subalkaline dykes are enriched compared to tholeiites with respect to light and middle REE, and depleted with respect to heavy REE; rocks of all groups have about the same concentration of Ho. No kimberlitic rocks display a Eu anomaly, whereas all rocks show strong negative Cs, K, Sr and Hf–Zr anomalies.

On a primitive-mantle-normalized spidergram kimberlites demonstrate an extremely high enrichment of the most incompatible elements – their concentrations vary from 100 to 700–800 times that of the primitive mantle norm. Normalized abundances gradually decrease as the degree of incompatibility of elements decreases. High-Ti subalkaline rocks are less enriched in incompatible elements: concentrations of the most incompatible elements vary from 50 to 100 times that of the primitive mantle, and gradually decrease towards less incompatible elements. Negative spikes of Cs, K and Sr are also pronounced in these rocks, but may be absent in some samples. In contrast to kimberlites, the negative spike of Hf–Zr is completely absent. Tholeiite dolerites have a rather flat pattern of trace elements – their abundances vary from 20 to 8 times that of the primitive mantle norm, with exceptions of Ba and Pb that are more abundant. Tholeiites show relatively weak negative anomalies of Cs, Th, U and Nb (but not Ta). As evident from spidergrams, concentrations of incompat-

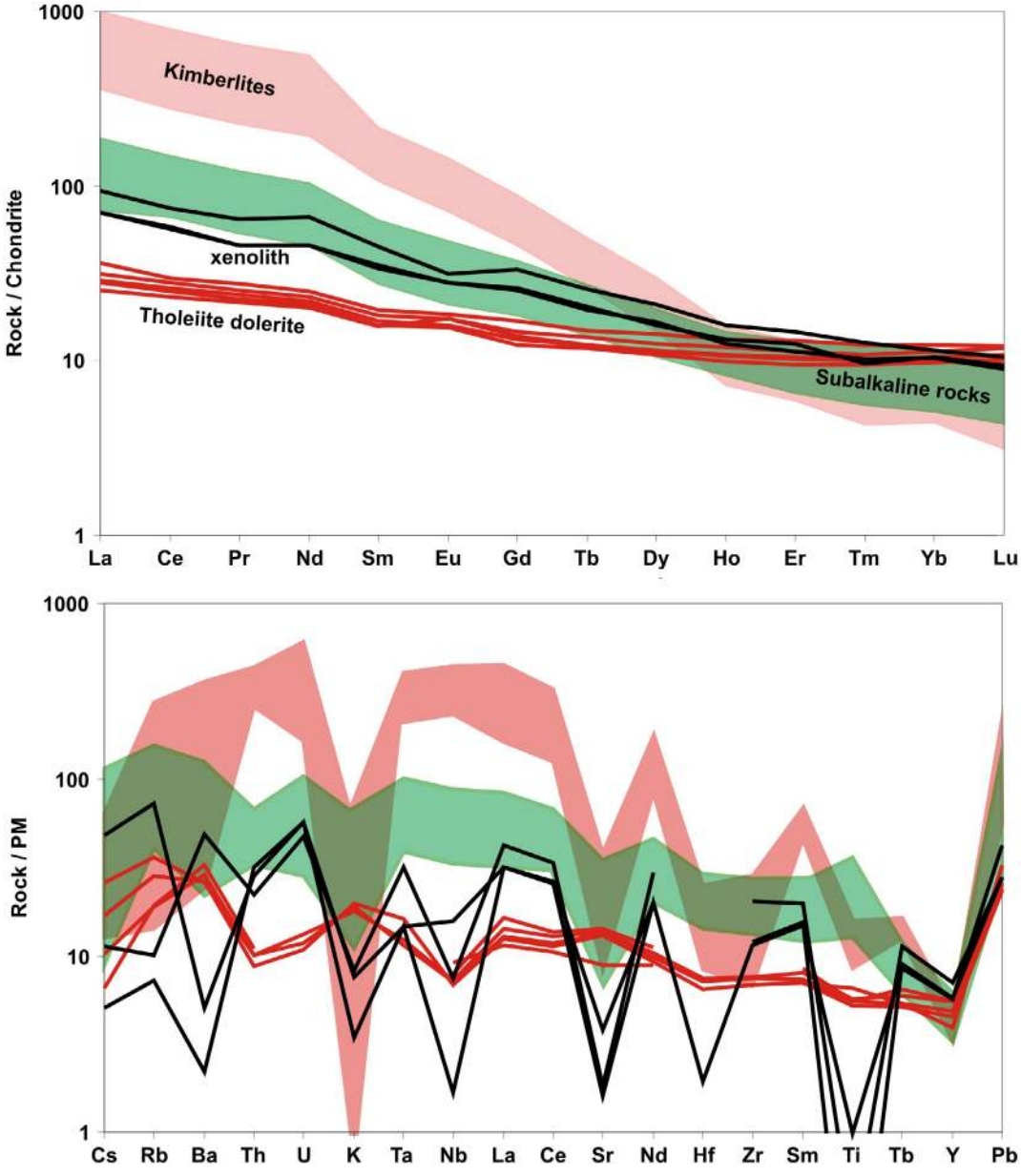

Fig. 3. Chondrite-normalized [according to Taylor and McLennan (1985)] REE distributions and primordial mantle-normalized [according to McDonough et al. (1992)] trace element distributions in dykes of the Ingul terrain of the Ukrainian shield (chemical analyses from Bogdanova et al., 2013, and new analyses by the authors).

Table 2. Sr, Nd and Pb isotope composition of mafic dykes and mantle xenolith in kimberlites, Ingul terrain of the Ukrainian shield.

Sample	Sm	Nd	$^{147}Sm/^{144}Nd$	$^{143}Nd/^{144}Nd \pm 2\sigma$	$^{143}Nd/^{144}Nd_{(1800)}$	εNd_{1800}	Rb	Sr	$^{87}Rb/^{86}Sr$	$^{87}Sr/^{86}Sr \pm 2\sigma$	$^{87}Sr/^{86}Sr_{(1800)}$	εSr_{1800}	$^{206}Pb/^{204}Pb$	$^{207}Pb/^{204}Pb$	$^{208}Pb/^{204}Pb$
1	1.86	11.43	0.0982	0.511603 ± 11	0.510441	2.6	46.4	33.8	4.0089	0.803241 ± 12	0.69946	–44	37.065	16.971	43.348
2							6.4	38.7	0.4789	0.716104 ± 10	0.70371	17	23.259	16.210	45.282
3	23.41	158.08	0.0895	0.511496 ± 5	0.510436	2.5	160.9	788.0	0.5914	0.718674 ± 9	0.70336	12	25.820	16.347	54.309
4	22.41	166.36	0.0814	0.511415 ± 4	0.510451	2.8	59.6	243.7	0.7088	0.725563 ± 10	0.70721	67	25.284	16.483	45.444
5	7.42	35.22	0.1274	0.511878 ± 6	0.510370	1.2	30.3	555.3	0.1579	0.707348 ± 8	0.70326	11	17.794	15.693	38.396
6	11.57	58.99	0.1186	0.511773 ± 5	0.510368	1.2	70	747.6	0.2710	0.710246 ± 13	0.70323	10	19.99	15.952	40.117
7	3.35	13.20	0.1535	0.512172 ± 4	0.510355	0.9	12.1	287.1	0.1219	0.706677 ± 16	0.70352	14	18.768	15.620	38.308
8	3.63	14.18	0.1548	0.512176 ± 4	0.510343	0.7	23.1	279.6	0.2391	0.708927 ± 17	0.70274	3	18.515	15.596	38.196
9	3.78	15.06	0.1518	0.512148 ± 8	0.510351	0.8	12.3	300.5	0.1184	0.706872 ± 11	0.70381	19	18.992	15.548	37.906
10	8.0	34.0	0.1423	0.511984 ± 4	0.510299	–0.2	1.4	249.1	0.0163	0.718487 ± 10	0.71807	222	33.249	17.399	40.894

Note: Key to samples: 1 – 4097-V-269.6, xenolith of peridotite in kimberlite; 2 – 4097-X-354.5, xenolith of spinel peridotite in kimberlite; 3 – 4095-III-312.9, xenolith of peridotite in kimberlite; 4 – 4097-VII-319.8, kimberlite; 5 – 72/170, subalkaline dolerite; 6 – 1420/343.4, subalkaline dolerite; 7 – 3424–287.4, dolerite; 8 – 3419–212.5, dolerite; 9 – 3417–45.3, dolerite; 10 – 06-BG21, dolerite.

ible trace elements decrease from kimberlites through high-Ti subalkaline rocks to tholeiites. The same can be said with respect to the compatible trace elements – Ni and Cr.

Isotope composition

Strontium, Nd and Pb isotope compositions were measured in 10 samples that include 3 mantle xenoliths in kimberlite, 1 kimberlite rock, 2 subalkaline mafic rocks and 4 tholeiite dolerites (Table 2). In spite of a large variability of studied lithologies and their partly altered nature, these display similar isotope systematics with tendencies for analytical data to define linear relationships. For instance, eight samples (a highly altered dolerite sample, 06-BG21, is excluded) can be fitted to a Sm–Nd regression (MSWD = 0.92, Fig. 4) that yields an age of 1566 ± 95 Ma with an initial $^{143}Nd/^{144}Nd = 0.510571 \pm 79$ ($\varepsilon Nd = -0.8$). This age is about 200 myr younger than the expected age of the rocks, so the εNd value based on the isochron age is considerably lower than individual εNd values calculated at e.g., 1800 Ma, an age consistent with field relationships and radiometric data presented in this study. However, it seems more sensible to consider isotope data representing groups of samples with similar chemistry. Despite the existence of more or less severe alteration features, it is shown in Fig. 4 that three straight-lines, equal to 1.78 Ga isochrons, can be reasonably well fitted to data points representing each of the identified rock types. This is apparently suggesting that the different lithologies could represent Sm–Nd systems which have stayed approximately closed on a whole-rock scale. Although there is a limited spread in Sm–Nd data and only few available analyses, the tentative development of discrete linear arrays in Fig. 4 is corroborated by the observation that each rock type appears to define its own εNd_{1800} signature (Table 3). In general, εNd_{1800} values vary in studied rocks from 0.7 to 2.8, with the highest values obtained for mantle xenoliths and their host kimberlite; these latter values are considerably lower than those which can be expected for the contemporaneous depleted mantle (DePaolo, 1981).

There is also a tendency for Rb–Sr data to define straight-line relationships (Fig. 4). Commonly, the Rb–Sr system does not remain closed subsequent to the time of rock emplacement. Three samples, including the highly altered dolerite (06-BG21), a kimberlite (4097-VII-319.8), and a peridotite xenolith from the same drill core (4097-VII-319.8), have variable initial Sr isotope ratios, but the remaining seven specimens display consistent initial (t = 1800 Ma) Sr isotope ratios that are close to 0.703. It is noteworthy that no systematic difference of $^{87}Sr/^{86}Sr_{1800}$ values can be seen between mantle xenoliths, subalkaline rocks and tholeiite dolerites. A straight-line defined by the eight samples corresponds to an age of 1729 ± 20 Ma, with an initial $^{87}Sr/^{86}Sr = 0.70366 \pm 41$ (MSWD = 10.8), that still is in agreement with field constraints. This regression due to the high MSWD cannot be regarded as a true isochron, but it still can serve as indication of the similarity of three groups of dykes in terms of their ages and initial Sr isotope compositions.

The Pb isotope data scatter significantly and the data points do not form any well defined linear arrays (Fig. 5). Yet, by checking the possibility of fitting data to a 1.8 Ga isochron, it appears that four data points (the two sub-alkaline dykes, the kimberlite and the altered dolerite; 06-BG21) give a decent fit (1793 ± 160 Ma, MSWD = 15). The other dolerites cluster in a position below

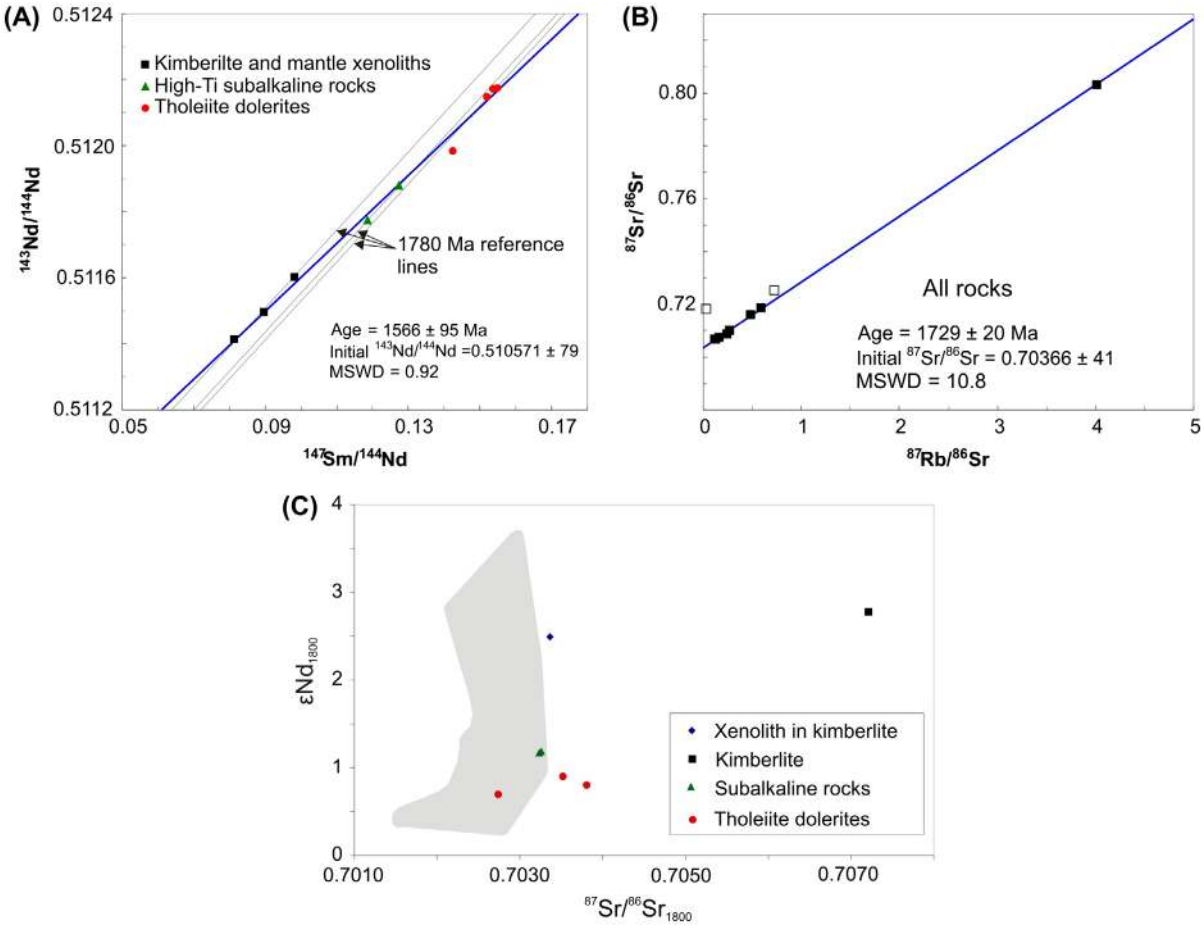

Fig. 4. Sm–Nd (**A**) and Rb–Sr (**B**) isochron diagrams and $^{87}Sr/^{86}Sr_{1800}$ versus εNd_{1800} plot (**C**) for dykes and xenoliths in kimberlites of the Ingul terrain of the Ukrainian shield. Empty box in (**B**) indicate sample that was not used for the isochron calculation, whereas shaded area in (**C**) indicates isotope compositions of contemporaneous tholeiite dykes of the North-Western region of the Ukrainian shield (data for the North-Western region is from Shumlyanskyy (2008) and Bogdanova et al. (2013)).

the four-point linear array, whilst the three xenoliths hosted by kimberlites exhibit highly variable Pb isotope compositions. Two samples (one of the xenoliths and the altered dolerite) have $^{206}Pb/^{204}Pb$ ratios exceeding 30 implying a considerable *in situ* growth of uranogenic lead (requiring an elevated U/Th ratio in rocks) after rock crystallisation. If it is assumed that ~1.8 Ga samples represent closed isotope systems and a narrow range of emplacement ages, then it can be deduced that rocks must be characterized by a range in their initial Pb isotope ratios.

Geochronology

Geochronological data regarding dykes of the Ingul terrain are scarce. These include a K–Ar age at 1900 Ma for phlogopite separated from a mica-bearing picrite (Nikolsky 1974), and several whole-rock K–Ar dates that vary from 1100 to 1700 Ma (Hrechishnikov et al. 1980). A 1800 Ma age for kimberlite dykes using the K–Ar method was quoted by Tsymbal et al. (1999), whereas Yutkina et al. (2005) applied the Rb–Sr method to establish a 1770 ± 9.4 Ma age of the Kirovograd kimberlites. Shumlyanskyy et al. (2010) reported U–Pb SIMS results of zircons from a dolerite dyke exposed in the Subotsy quarry that yielded an age of 1774.3 ± 7.4 Ma. Finally, Tsymbal et al. (2011) quoted results of U–Pb zircon dating of two mafic dykes: one dyke associated with kimberlites near city of Kirovograd defined ages in the range 2056–2046 Ma, whereas another dyke located some 50 km eastwards yielded zircon ages from 2074 to 2041 Ma. We interpret these zircons as inherited from granitic rocks that are widely distributed in the area (Fig. 1).

In order to better constrain the age of the mafic dyke magmatism in the Kirovograd area we sampled one dolerite dyke (sample 1098) within the Lelekivka kimberlite field (Fig. 1). Only a few zircons grains could be separated, and these are prismatic, c. 0.1 mm × 0.3 mm in size, with poorly developed di-pyramidal facets. Grains are euhedral, colourless, transparent and contain numerous fine inclusions. Cathodoluminescence imaging reveals simple zonation (Fig. 6). Four individual U–Pb single-grain analyses were carried out (Table 3), and two of the analyses are 100% concordant, the third is 99% and the fourth is 97% concordant. The concordia age is 1810 ± 15 Ma (Fig. 7), and is interpreted to date the emplacement of the dyke. Other possibility is that these zircons could have been captured from the wall rocks as may be suggested from their slightly variable appearance and rounded crystal shape. However, we regard this possibility as unlikely as host rocks of this age are unknown in the area.

Table 3. Results of U–Pb LA-ICP-MS dating of zircons from the dolerite sample 1098.

Spot #	Conc., ppm		Th/U	Isotope ratios							Age, Ma ± 2σ		Conc %
	U	Pb		$^{206}Pb/^{204}Pb$	$^{206}Pb/^{238}U$	2σ, %	$^{207}Pb^{235}U$	2σ, %	$^{207}Pb/^{206}Pb$	2σ, %	Rho	$^{206}Pb/^{238}U$	$^{207}Pb^{235}U$	$^{207}Pb/^{206}Pb$	
a34	118	39	0.13	5959	0.32274	2.3	4.9016	3.0	0.11015	2.0	0.76	1803 ± 36	1803 ± 26	1802 ± 36	100
a35	57	21	0.44	27801	0.32475	2.8	4.9450	5.4	0.11044	4.6	0.52	1813 ± 44	1810 ± 46	1807 ± 83	100
a36	39	15	0.54	2998	0.32397	1.8	4.9663	3.2	0.11118	2.6	0.58	1809 ± 29	1814 ± 27	1819 ± 47	99
a38	102	35	0.21	8872	0.32643	3.0	5.1801	8.4	0.11509	7.9	0.36	1821 ± 48	1849 ± 74	1881 ± 142	97

Discussion

Origin of initial melts

An abundant mantle melting can be explained by three scenarios (e.g., Ernst 2014, and references therein): elevated water content, a drop in pressure (decompression), and an increase in mantle temperature. Among all these scenarios an increase of mantle temperature is the only substantial possibility in the intraplate setting (see Ernst 2014, for discussion). There are evidently several viable mechanisms that can cause a thermal anomaly 50–200 °C above ambient mantle temperatures that is required for onset of melting. If bolide impact and processes related to the plate-boundary processes are excluded, then two main possible mechanisms that are able to entail melting remain, namely: different varieties of the mantle plume model, and delamination of lithosphere. The mantle plume model foresees an upward movement of a large mass of hot mantle material. As it reaches the base of the lithosphere, it starts to spread beneath the lithosphere, causing domal uplift and extension of lithosphere that eventually may lead to rifting. All these factors cause melting of the plume, and, possibly, lithospheric material. In the second model the delamination of lithosphere causes upward flow of asthenospheric material into the lithospheric hole that appeared due to delamination. This asthenospheric material can melt adiabatically during descent. In the case of the Ukrainian shield the delamination might have been caused by collision of Sarmatian and Fennoscandian segments of the East-European platform which occurred shortly before 1800 Ma (Bogdanova et al. 2008).

There are several diagnostic characteristics of plume involvement (Ernst 2014), that include, among others: ocean-island basalt (enriched) composition, depth range of melting, high degree of melting and presence of high-Mg melts. The plume-related magmatism usually span less than 10–15 myr and in many cases rocks are emplaced in only a few myr or less (see Ernst 2014, and references therein), that makes distinguishing of several pulses of magmatism especially hard task.

The three groups of dykes, defined above, demonstrate significant differences in their geochemical composition and do not form continuous trends in chemical variation diagrams (Fig. 2). Therefore, these groups of dykes are not thought to be related to each other by fractional crystallization of a single initial melt, but were probably derived from different sources. Whereas geochemical data indicate certain variability in the sources for magmas generating the different dyke types, the isotope data instead reflect overall similarities in their magma sources.

Before evaluating the significance of the radiogenic isotope data it necessary to clarify whether isotope data are reflecting primary, unaltered conditions and, if so, may be modelled by a single stage evolution, or whether they are significantly affected by secondary processes. The calculated nine-point Sm–Nd isochron age of 1.56 Ga is essential in this respect. There is no field evidence arguing for any kind of post-1.75 Ga geological event to have affected the country rocks, and neither are there any isotope data from wall rocks in the Ingul Domain indicating a 1.56 Ga event. The relatively uniform εNd_{1800} values for the respective dyke type and the tendencies for isochrons to be developed in all of the studied isotope systems would support that isotope data are essentially consistent with a single stage evolution; 1800 Ma to the present time. The fact that there are secondary mineral parageneses, involving e.g., calcite, talc and serpentine, developed in different dykes, must also be considered. The lack

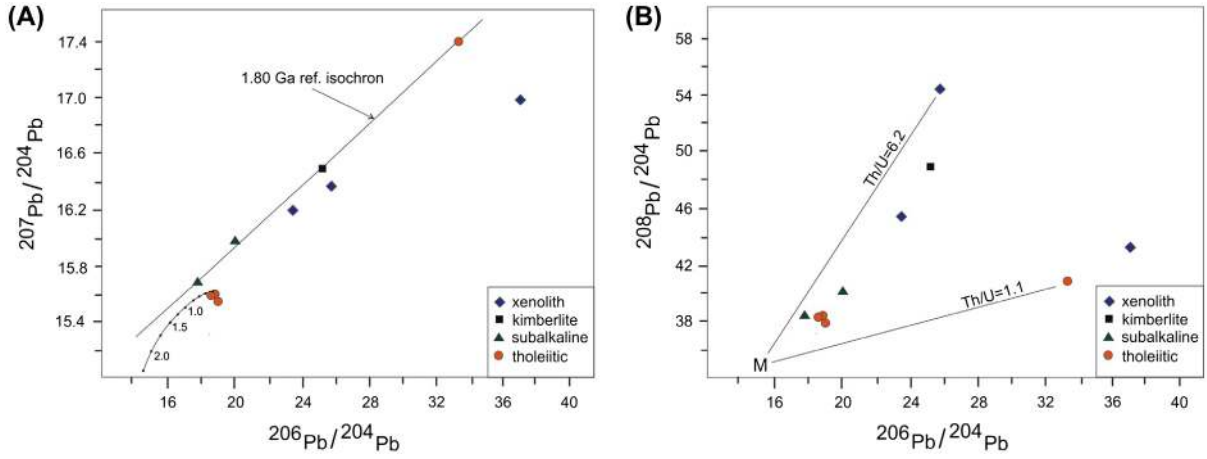

Fig. 5. Pb–Pb isotope diagrams. Added to panel **A** is part of the Stacey and Kramers (1975) two-stage evolution curve (tick marks are indicated for every 250 Ma). The symbol M in panel **B** denotes an approximate mantle composition at 1.8 Ga ($^{206}Pb/^{204}Pb$ = ca. 15.2 and $^{208}Pb/^{204}Pb$ = ca. 34.8) and is used to calculate crude Th/U ratios for the investigated rocks.

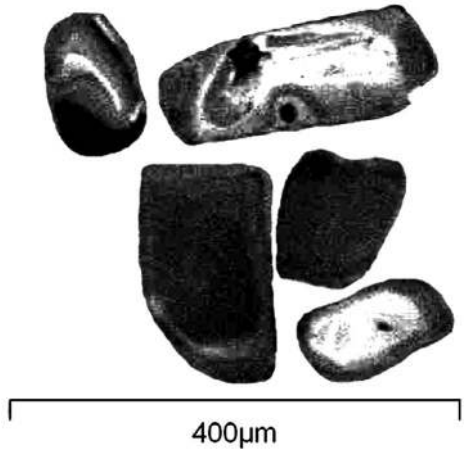

Fig. 6. CL image of zircons isolated from the dolerite sample 1098.

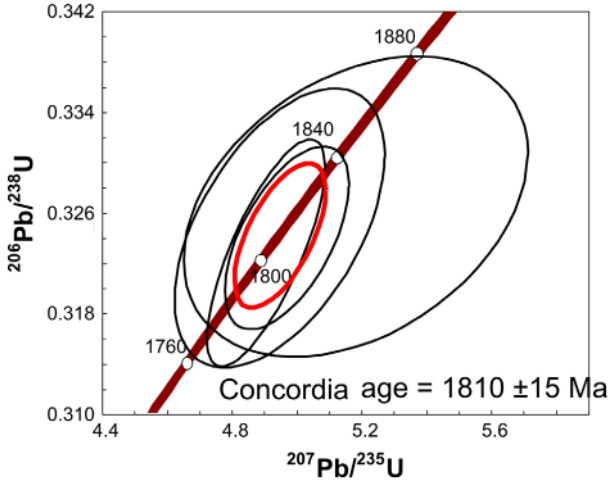

Fig. 7. U–Pb concordia diagram for zircons from dolerite sample 1098.

of geological and isotope evidence for the existence of a post-1.75 Ga event would imply that it is most likely that secondary mineral formation is linked to a late stage of the magmatic evolution. It is possible that a secondary alteration of rocks took place as part of the regional metasomatism that apparently occurred between 1.8 and 1.75 Ga. The elevated uranogenic Pb isotope ratios of several samples would be given a reasonable explanation if uranium was added to rocks in connection with metasomatism. The development of secondary mineral assemblages and possible interaction with external fluids may have led to some influence on the isotopic systems, but this effect is probably minor given that the volumetrically dominant primary mineral phases are likely to control the bulk isotope budgets, and therefore the obtained whole rock isotope composition. Nonetheless, there are apparent distinctions between isotopic systems and an example is given by one dolerite (3417–45.3) which shows similarities with the three other analysed dolerites with respect to the Rb–Sr and Sm–Nd system but deviates in the Pb–Pb system. Although it is important to avoid putting too much weight on results for single samples, calculated or inferred (Pb–Pb system) initial isotope compositions may be used to shed further light on the source of rock-forming magmas. The noted scatter in isotope data, leaving out the samples with geologically unlikely initial Sr isotope ratios, would then basically reflect isotope heterogeneities in newly crystallized rocks some 1.8 Ga ago. Likewise, the enriched chemical nature of rocks is interpreted as a primary feature and not as a result of sub-solidus alteration processes.

The samples forming part of this study are petrologically and chemically different, and are sampled within a large region, and a perfect linear alignment of all samples in isotopic diagrams is hardly an expected feature. Still, a linear alignment in Sm–Nd and Rb–Sr isochron diagrams indicates that involved magma sources had broadly similar isotopic characteristics. Uniform $^{87}Sr/^{86}Sr$ initial ratios (1800 Ma) of around 0.703 for most samples, and initial Nd isotope ratios between c. +1 to +3 seem to suggest a mildly depleted source rather than indicating a depleted mantle origin. Pb isotope data also indicate a relatively enriched source for certain samples. This is based on a comparison between the linear array displayed in Fig. 5 and the isotope composition of average crustal lead according to the Stacey and Kramers (1975)

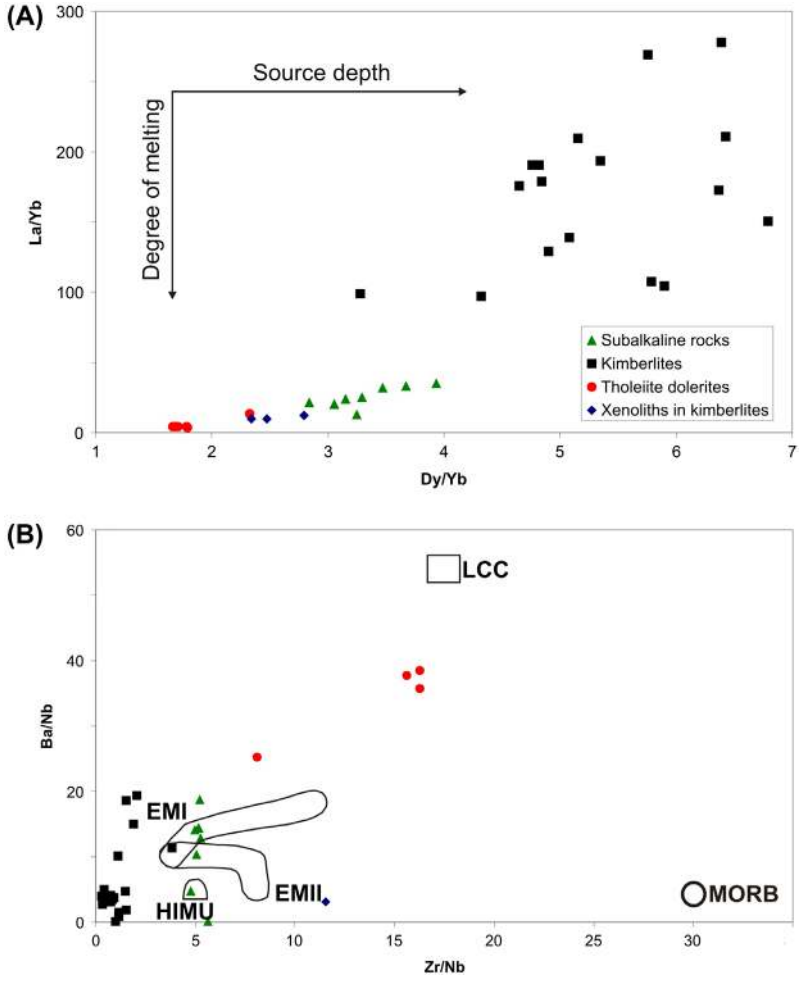

Fig. 8. Dy/Yb versus La/Yb (**A**) and Zr/Nb versus Ba/Nb (**B**) plots for dykes and xenoliths in kimberlites of the Ingul terrain of the Ukrainian shield. **A**. The increase in Dy/Yb reflects the increased depth of melting and decreasing La/Yb reflects an increase in the amount of partial melting (Riley et al., 2005). This is because Dy/Yb ratio is determined by the amount of garnet in the mantle restite which is thought to increase with depth causing the more fractionated REE pattern (higher Dy/Yb) in the equilibrium melt. At the same time, partition coefficients for light REE in garnet and most other fusible minerals in equilibrium with mafic melts is less than 1. So, light REE will preferentially be partitioned into the melt at the very low degrees of melting, causing high La/Yb; as degree of melting increases, involvement of olivine in the melting will cause decrease in La/Yb. According to our data, tholeiite dolerites were formed at shallower depth and higher degree of melting, in contrast to kimberlites that originated due to low-degree melting at great depth. **B**. Abbreviations for reservoirs: LCC – Lower Continental Crust; MORB – Mid-Ocean Ridge Basalts; EMI – Enriched Mantle type 1; EMII – Enriched Mantle type 2; HIMU – reservoirs with highly radiogenic Pb isotope ratios (high μ). The Zr/Nb and Ba/Nb values are according to Weaver (1991) (MORB, EM and HIMU) and Rudnick and Gao (2003) (LCC). Zr/Nb ratio varies opposite to La/Yb, i.e. increases as degree of melting increases. This is due to the much higher partition coefficients for Nb than for Zr (Kamber and Collerson, 2000). As a result, the low-degree melts contain a lot of Nb, leaving a residue depleted in Nb and still relatively rich in Zr. As melting proceeds, the residue continues to supply Zr that results in a gradual increase of Zr/Nb. Ba/Nb is high in the continental crust and is a good proxy of crustal contamination. Kimberlites and subalkaline high-Ti rocks plot close to the enriched mantle fields, indicating their enriched source, in contrast to the depleted mantle source of the MORB. The tholeiitic dolerites are displaced towards the lower crustal value that evidences about the lower-crustal contamination.

two-stage evolution model ($\mu^2 = 9.74$) for terrestrial lead. If this linear array is extrapolated towards less radiogenic values, it is seen to pass above the point representing 1750 Ma in the Stacey and Kramers (1975) model. This relationship implies that the source of ≥1.75 Ga magmas representing data points on the linear array must have had an evolved μ^2 value that is well above any typical value for a depleted mantle.

Geochemical data indicate that an initial kimberlite melt is a product of low-degree melting of a garnet-bearing mantle peridotite at great depth, in the lower part of the subcontinental lithospheric mantle. On the Ba/Nb–Zr/Nb diagram (Fig. 8) the high-Ti subalkaline dykes plot close to the enriched mantle sources (HIMU and EM) that probably indicate their derivation directly from material of the mantle plume. On the same diagram, kimberlites are displaced towards low Ba/Nb and Zr/Nb values that are due mainly to the very high concentrations of Nb in the Kirovograd kimberlites. To explain the extremely high concentration of incompatible trace elements in kimberlitic melts we have to accept a very low (fractions of a percent) degree of selective partial melting of the enriched plume material.

As can be seen from the Ba/Nb versus Zr/Nb plot (Fig. 8), tholeiite dolerites are displaced towards the area defined by lower crustal values. This indicates an involvement of lower crustal components during melting processes that created the initial tholeiitic melts. Also the negative Nb–Ta anomaly visible in these rocks (Fig. 3) supports some influence of crustal material on the tholeiitic chemistry. It is further inferred from the Dy/Yb versus La/Yb plot (Fig. 8) that there is a gradual change in the degree of melting characterizing different dyke types, with kimberlitic melts produced by a low-degree fusion at great depths in contrast to more pronounced melting at shallower depths leading to formation of tholeiitic melts. This diagram, however, cannot be used to set any constrains on the temporal evolution of the sequential melting process. Given the current lack of precise ages, it remains an open question if the zone of partial melting ascended from a sub-lithospheric depth to the lower-crustal level with corresponding increase of the degree of melting, or if a reverse process took place; i.e. a progressive deepening of the melting site which was accompanied by a decrease of the degree of melting.

Even if the obtained isotope data are reflecting the true isotopic signatures at the time of crystallisation, it is not self-evident that such signatures are properly revealing the isotopic features of the initial melts. Kimberlitic magmas are known to frequently assimilate higher-level crustal material during ascent, xenoliths are obviously not representative of an initial melt, and for instance the dykes dated by Tsymbal et al. (2011) in the Ingul Domain carried inherited zircons which is suggesting an assimilation of locally available crustal rocks. Although there is no obvious relation between εNd (and initial Sr and Pb isotope

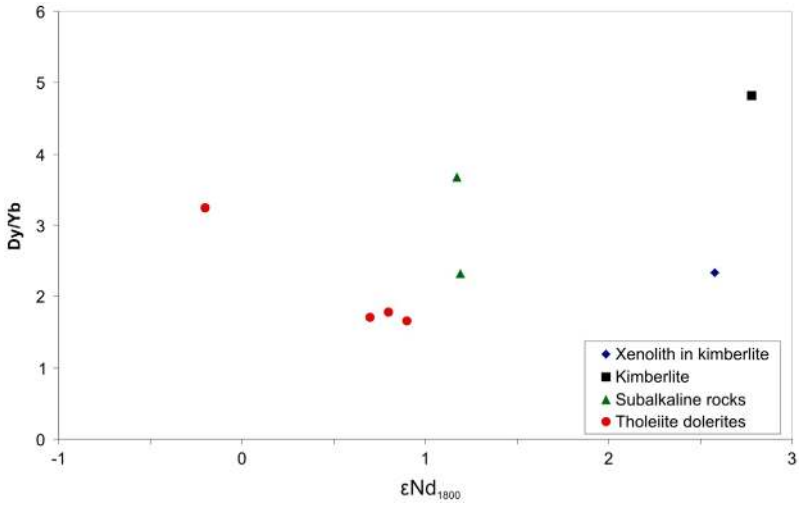

Fig. 9. εNd_{1800} versus Dy/Yb plot that demonstrates relationships of Nd isotope composition with depth of the source (see Fig. 8), and shows gradual depletion of the source with increase of its depth.

compositions) and La/Yb, a weak dependence on the Dy/Yb ratio may be discerned (Fig. 9). This may indicate that the degree of partial melting was not the main factor controlling the isotopic composition of the melts, but the possibility of crustal assimilation during ascent makes it impossible to draw any firm conclusions. Additional isotope work, also including mineral separates, will be needed in order to advance the understanding about variations in Sr, Nd and Pb isotope compositions and whether or not these are reflecting real isotopic variation in the lithosphere's vertical section, or if they simply are a function of the degree of crustal contamination. It appears possible, however, on the basis of Pb isotopes and the assumption that no lead mobilisation affected rocks after their crystallisation, that ascending magmas must have interacted both with upper crustal (cf. samples on the linear array) and lower crustal lithologies (cf. the retarded $^{207}Pb/^{204}Pb$ value of the kimberlite). The large range in calculated Th/U ratios (Fig. 5) cannot be linked to magma characteristics as such ratios obviously could be affected by a U metasomatic event, and therefore the obtained $^{208}Pb/^{204}Pb$ ratios of rocks probably are a combined result of crustal assimilation and late-stage alteration influencing the primary melt compositions. It may also be noted that the xenoliths in kimberlite are isotopically distinct from each other and also different from the kimberlitic signature suggesting that xenoliths were assimilated at different depths and from isotopically different rocks.

High-Ti subalkaline and low-Ti tholeiitic melts

There is a clear division of effusive rocks in many LIPs into high-Ti and low-Ti subtypes. Rocks that belong to the high-Ti subtype are regularly enriched with respect to incompatible elements and demonstrate more fractionated REE pattern as compared to their low-Ti counterparts. Moreover, these two subtypes can be spatially detached and either occur in separate areas or constitute different parts of a vertical rock section (e.g., Ernst 2014, Section 10.5.3). As an example, effusive rocks of the Vendian Volyn flood basalt province located at the western slope of the Ukrainian shield can be divided into low-Ti and high-Ti subtypes, with the latter being significantly enriched in incompatible trace elements and having a fractionated REE patterns (Shumlyanskyy2012). The high-Ti basalts occur exclusively in the top part of the flood basalt sequence and are separated from its main part by an unconformity.

There are two main hypotheses that attempt to explain the origin of these two types of melts; (i) chemically distinct melts develop as a result of different degrees of partial melting of the mantle material (Peate 1997). This is explained either (1) by assuming that the distance from the axial part of the mantle plume is crucial; low-Ti melts develop due to a high degree of melting in the hot axial part of the plume, while high-Ti melts form at lower degrees of melting in the colder peripheral areas (Fodor 1987); or (2) by arguing that the difference in the lithosphere thickness controls the degree of melting of the sublithospheric asthenosphere. According to this model, the degree of melting beneath the thick lithosphere is very limited and occurs in the presence of residual garnet that results in the formation of high-Ti melts enriched in incompatible elements. A more shallow fusion beneath the thin lithosphere within the stability field of spinel leads to a larger degree of melting and the equivalent melt corresponds to low-Ti basalts (Arndt et al. 1993); (ii) variable melt compositions are thought to be related to differences in the chemical composition of the mantle sources (Arndt and Christensen 1992; Peate and Hawkesworth 1996; Smithies et al. 2005), or melt compositions are controlled by differences in the chemical composition of the lithospheric mantle (Gibson et al. 1996; Peate 1997) which is believed to serve as a source for the initial melts or act as a contaminant of the sublithospheric mantle melts.

There are no systematic variations in Nd, Sr and Pb isotopic composition between low-Ti and high-Ti rocks in the Ingul Domain which can help in understanding their origin, and basically different rock types may plot on common linear arrays. Tentatively, this is advocating for a gross isotopic similarity between sources representing different levels in the mantle-crust cross-section, and for a limited assimilation of isotopically distinct material. An alternative explanation where contamination processes causes a broad isotopic similarity of rocks that originally had quite contrasting isotopic signatures appears less likely. With this in mind, the geochemical features for the different dyke types may indicate a different extent of melting of the same (or similar) material at different depths, with a limited lower crustal contamination in the case of low-Ti tholeiites. One point to also keep in mind is that although

the three groups of Ukrainian dykes are spatially juxtaposed, tholeiitic melts can be transported laterally for hundreds and even more than a thousand kilometres away from a plume source (Ernst 2014). However, kimberlite dykes are emplaced mostly vertically. In such a scenario, the source mantle for the tholeiitic dykes could be hundreds of km away or more (where the lithosphere is already thinned) from the present site, while the kimberlites are being vertically emplaced from regions located beneath thicker lithosphere. An analogue is the Deccan volcanism that extends for at least 800 km into eastern India reaching the area of the Bastar craton. The feeder system of dykes can be traced eastwards for more than 600 km along the Narmada-Tapti rift from the Deccan plume centre on the western side of India. Coeval kimberlites are found in the Bastar craton on the eastern side of the Indian craton nearly 800 km from the plume centre (e.g., Lehmann et al. 2010). Tentatively, these tholeiite dykes were generated from sources beneath a lithosphere that might have become thinned due to material removal by the Deccan plume, whilst the kimberlites were generated from a portion of the plume head that extended beneath the thick lithospheric root of the Bastar craton 800 km to the east. The possibility of a distal transportation of the tholeiitic melts does not preclude the mantle plume model, but rather prompts similarity in isotope compositions of melts spatially juxtaposed at the surface.

Relation to the 1790–1780 Ma Ni-rich dykes of the North-Western region of the Ukrainian shield

Numerous dykes of Ni-rich tholeiitic dolerites, as well as several layered 1.79–1.78 Ga gabbroic intrusions are widely distributed within the North-Western region of the Ukrainian shield (Shumlyanskyy et al. 2012; Bogdanova et al. 2013; Shumlyanskyy et al., this volume). Dykes of sub-alkaline gabbro and alkaline ultramafic intrusions of presumably the same age are also known. The newly obtained U–Pb age for the dolerite dyke in the Kirovograd area confirms a wide geographical distribution of this ca. 1790–1780 Ma magmatic event within the Ukrainian shield and adjacent Voronezh massif. Thus, this Palaeoproterozoic LIP embraced large regions of Sarmatia and included a wide range of the mantle-derived melts.

Currently, the studied Ingul kimberlite and high-Ti subalkaline groups of dykes are not known to have any counterparts in the North-Western region of the Ukrainian shield. However, as noted above, tholeiitic dolerites are widely distributed in the North-Western region and there is a geochemical similarity between tholeiitic dolerites in these two regions (Figs. 2 and 3). The main difference is a lower concentration of Ni (c. 40 ppm) in tholeiites of the central part of the Ukrainian shield compared to corresponding rocks in the North-Western region (c. 90 ppm), although some low-Ni tholeiite dykes of this age are also found in the latter area.

Low-Ti tholeiite dykes in the both regions of the Ukrainian shield reveal similar Sr and Nd isotope composition (Fig. 4), although on the average the tholeiites of the North-Western region have more radiogenic Nd and less radiogenic Sr isotope composition. Part of the difference in the Sr isotopic signature may be due to open Rb–Sr systems (elevated, calculated initial Sr rock values result from a partial Rb loss). Yet, certain differences in isotopic character between regions are probably explained by the crust in the central part of the Ukrainian shield being overall older and with a less radiogenic Nd and more radiogenic Sr isotope composition compared to the crust in the North-Western region. Nonetheless, tholeiites in both areas of the Ukrainian shield are similar in terms of age and chemical and isotope composition, and we consider that these rocks belong to the same igneous event and represent parts of a single Palaeoproterozoic LIP.

Taking into account the wide spatial distribution of the mantle-derived rocks, their geochemical composition indicative of a mantle source enriched in incompatible elements in relation to the source of mid-ocean ridge basalts, and a wide range of melt compositions formed at different depths, we assume that melting was caused by a mantle plume. In favour of this hypothesis is the work by Cuney et al. (2012) who suggested that metasomatic activity in the Ingul terrain was triggered by the onset of a mantle plume. This assumption is supported by geophysical data reported by Kazansky (2013), and by spatial and secular coincidence of the mantle-derived dyke magmatism and metasomatic activity. A different explanation of origin of the Palaeoproterozoic dykes of the Ukrainian shield was presented by Bogdanova et al. (2013) who suggested that formation of the dykes was related to convergent tectonics and collisional orogeny due to oblique collision of the Volgo-Sarmatian and Fennoscandian segments of the East-European platform and subsequent rotation of the newly formed continental block.

Connection to the U deposits

Dyking in the Ingul terrain occurred nearly simultaneously with the formation of numerous U deposits related to albitites of metasomatic origin. Two efforts to date albititisation resulted in ages at 1818 ± 42 and 1808 ± 27 Ma (Scherbak et al. 2008). Uranium-bearing metasomatites cut across the Novoukrainka and Kirovograd granites and metamorphic rocks of the Ingul-Ingulets Series (Cuney et al. 2012). Their xenoliths were found in kimberlites and subalkaline rocks (Tsymbal 2013), whereas Zankevych et al. (2014) mentioned that some of the mafic dykes were affected by the Na metasomatism.

All U deposits are located within the Subotsy-Moshoryn tectonic zone, relatively close to the contact of the KNPC (Cuney et al. 2012). Besides albitites, this tectonic zone accommodates numerous mafic and ultramafic dykes. The U deposits are unknown within the KNPC, although small metasomatic bodies occur also in the extreme south-western part of the KNPC (Kalashnik and Moskalenko 2010), that may indicate a prolonged period of metasomatic activity. In any case, the location of the U mineralization is controlled by the same crustal structures that apparently also controlled the distribution of mafic and ultramafic dykes in the area (Kalashnik and Moskalenko 2010), and the ages of dykes and mineralizations are broadly similar.

Conclusions

A large number of mafic and ultramafic dykes widely varying in composition are known in the Palaeoproterozoic Ingul terrain, located within the central part of the Ukrainian shield. Geological relationships constrain the time of dyke emplacement to between c. 2020 and 1760 Ma, whereas scarce geochronological data indicate ages around 1800 Ma. These ages are in good agreement with ages of similar dykes which are widespread in the North-Western region of the Ukrainian shield.

Geochemical and petrographical data allow identification of three groups of dykes which are not related to each other by fractional differentiation of a single initial melt. The first group of dykes includes kimberlites that are the product of low-degree melting of a garnet-bearing mantle peridotite in the lower part of the subcontinental lithospheric mantle. Numerous xenoliths of peridotites hosted by kimberlites probably represent fragments of the mantle source. The second group of dykes includes high-Ti subalkaline mafic and ultramafic rocks that were probably derived from geochemically enriched source materials. Finally, the third group of dykes are tholeiite dolerites that bear a significant geochemical signal of lower-crustal contamination.

Taking into account the wide spatial distribution of the mantle-derived rocks, their geochemical composition indicative of enriched-mantle sources, and the wide range of melt compositions formed at different depths, we assume that melting was caused by a mantle plume. In this context, geochemical data indicate varying depths of partial melting for the different dyke groups, from sub-lithospheric (small degree of melting) to higher sub-crustal levels (higher degree of melting). The duration of the indicated progressive change of the locus of melting is not known, but a certain age difference (few myr) would be predicted between the different dyke types which all occur within a restricted region. As yet no radiometric data are available to set further time constraints on dyke emplacement. Additional insight into the differences in dyke chemistry within the mantle plume model is provided by the knowledge that doleritic dykes can be emplaced laterally for long distances (hundreds of kilometers or more) from the plume centre region, and from this follows that the source area for the dolerites can be distinct from that of the kimberlite dykes which are likely to be emplaced vertically.

Dyking in the Ingul terrain was closely associated in time and space with metasomatic albitites that host numerous economic U deposits. This association is apparently not accidental, and both dyking and metasomatism were likely related to the onset of a mantle plume.

Acknowledgements – This is publication No. 48 of the Large Igneous Provinces – Supercontinent Reconstruction – Resource Exploration Project (www.supercontinent.org NSERC CRDPJ 419503-11; www.camiro.org/exploration/ongoing-projects CAMIRO Project 08E03).

References

Arndt, N.T. & Christensen, U., 1992: The role of lithospheric mantle in continental flood volcanism: thermal and geochemical constraints. *Journal of Geophysical Research 97* (B7), 10967–10981.

Arndt, N.T., Czamanske, G.K., Wooden, J.L. & Fedorenko, V.A., 1993: Mantle and crustal contributions to continental flood volcanism. *Tectonophysics 223*, 39–52.

Bogdanova, S.V., Bingen, B., Gorbatschev, R., Kheraskova, T.N., Kozlov, V.I., Puchkov, V.N. & Volozh, Y.A., 2008: The East European Craton (Baltica) before and during the assembly of Rodinia. *Precambrian Research 160*, 23–45.

Bogdanova, S.V., Gintov, O.B., Kurlovich, D., Lubnina, N.V., Nilsson, M., Orlyuk, M.I., Pashkevich, I.K., Shumlyanskyy, L.V. & Starostenko, V.I., 2013: Late Palaeoproterozoic mafic dyking in the Ukrainian Shield of Volgo-Sarmatia caused by rotation during the assembly of supercontinent Columbia (Nuna). *Lithos 174*, 196–216.

Bryan, S.E. & Ernst, R.E., 2008: Revised definition of Large Igneous Provinces (LIPs). *Earth-Science Reviews 86*, 175–202.

Carignan, J., Hild, P., Mevelle, G., Morel, J. & Yeghicheyan, D., 2001: Routine analysis of trace elements in geological samples using flow injection and low pressure on line liquid chromatography coupled to ICP-MS: a study of geochemical reference materials BR, DR-N, UB-N, AN-G and GH. *Geostandards and Geoanalytical Research 25*, 187–198.

Claesson, S., Bibikova, E., Shumlyanskyy, L., Dhuime, B. & Hawkesworth, C., 2015: The oldest crust in the Ukrainian shield – Eoarchaean U–Pb ages and Hf–Nd constraints from enderbites and metasediments. *In* N.M.W. Roberts, M. Van Kranendonk, S. Parman, S. Shirey, & P.D. Clift (eds): *Continent formation through time*, 389, 227–259. Geological Society, London.

Cuney, M., Emetz, A., Mercadier, J., Mykchaylov, V., Shunko, V. & Yuslenko, A., 2012: Uranium deposits associated with Na-metasomatism from central Ukraine: a review of some of the major deposits and genetic constraints. *Ore Geology Reviews 44*, 82–106.

Cuney, M., Scherbak, M.P., Emetz, A.V., Petrychenko, K.V. & Sinelu, S., 2008: Petrological and geochronological peculiarities of Novoukrainka massif rocks and age problem of uranium mineralization of the Kirovograd megablock of the Ukrainian shield. *Mineralogichny Zhurnal 30* (2), 5–16.

De Ignacio, C., Muñoz, M., Sagredo, J., Fernández-Santín, S. & Johansson, Å., 2006: Isotope geochemistry and FOZO mantle component of the alkaline–carbonatitic association of Fuerteventura, Canary Islands, Spain. *Chemical Geology 232*, 99–113.

DePaolo, D.J., 1981: Neodymium isotopes in the Colorado Front Range and crust–mantle evolution in the proterozoic. *Nature 291*, 193–196.

Elming, S.-Å., Shumlyanskyy, L., Kravchenko, S., Layer, P. & Söderlund, U., 2010: Proterozoic basic dykes in the Ukrainian shield: a palaeomagnetic, geochronologic and geochemical study – the accretion of the Ukrainian shield to Fennoscandia. *Precambrian Research 178*, 119–135.

Ernst, R.E., 2014. *Large igneous provinces*. Cambridge University Press, Cambridge. 653 pp.

Fodor, R.V., 1987: Low- and high-TiO_2 flood basalts of southern Brazil: origin from picritic parentage and a common mantle source. *Earth and Planetary Science Letters 84*, 423–430.

Gerdes, A. & Zeh, A., 2006: Combined U–Pb and Hf isotope LA-(MC-) ICP-MS analysis of detrital zircons: comparison with SHRIMP and new constraints for the provenance and age of an Armorican metasediment in Central Germany. *Earth and Planetary Science Letters 249*, 47–61.

Gibson, S.A., Thompson, R.N., Dickin, A.P. & Leonardos, O.H., 1996: Mafic potassic magmatic key to plume-lithosphere interactions and continental flood-basalts. *Earth and Planetary Science Letters 141*, 325–341.

Hrechishnikov, N.P., Korzhneva, E.P., Kramar, O.A. & Scherbak, N.P., 1980: O vozraste dajkovykh porod Subbotsko-Moshorinskoj zony razlomov [On age of dykes of the Subotsy-Moshoryno fault zone]. *Geologichny Zhurnal 40*(5), 139–143 [In Russian].

Kalashnik, A.A. & Moskalenko, G.M., 2010: Geologo-strukturnye osobennosti prostranstvennogo razmescheniya kimberlitoproyavlenij I uranovorudnykh ob'ektov v Kirovogradskom rudnom rajone Ukrainskogo schita [Geological-structural peculiarities of spatial distribution of kimberlite occurrences and U mineralization in the Kirovograd ore district of the Ukrainian shield]. *Mineralni Resursy Ukrainy Iss 2*, 8–18 [In Russian].

Kamber, B.S. & Collerson, K.D., 2000: Zr/Nb systematics of ocean island basalts reassessed – the case for binary mixing. *Journal of Petrology 41*, 1007–1021.

Kazansky, V.I., 2013. Evolutsiya vzglyadov na metallogeniyu Kirovogradskogo rudnogo rajona [The evolution of views on the Kirovograd ore district metallogeny]. *In* V.I. Starostenko, & O.B. Gintov (eds.): *Kirovograd Ore District. Deep Structure. Tectonophysical Analysis. Mineral Deposits*, 327–337. Prastye Ludy Publisher, Kyiv [In Russian].

Krutikhovskaya, Z.A., Pashkevich, I.K. & Podolyanko, V.V., 1976: Zakonomernosti raspredeleniya dajkovykh kompleksov na Ukrainskom schite [Regularities of distribution of dyke complexes of the Ukrainian Shield]. *Geofizicheskij Sbornik 74*, 61–74 [In Russian].

Lehmann, B., Burgess, R., Frei, D., Belyatsky, B., Mainkar, D., Rao, N.V. & Heaman, L.M., 2010: Diamondiferous kimberlites in central India synchronous with Deccan flood basalts. *Earth and Planetary Science Letters 290*, 142–149.

McDonough, W.F., Sun, S.-S., Ringwood, A.E., Jagoutz, E. & Hofmann, A.W., 1992: Potassium, rubidium, and cesium in the Earth and Moon and the evolution of the mantle of the Earth. *Geochimica et Cosmochimica Acta 56*, 1001–1012.

Nikolsky, A.P., 1974: Slyudistye pikrity tsentralnoj tchasti Ukrainskogo schita [Micaceous picrites of the central part of the Ukrainian shield]. *Doklady Akademii Nauk SSSR 215*, 1451–1453 [In Russian].

Peate, D.W., 1997. The Paraná-Etendeka province. J.J. Mahoney & M.F. Coffin (eds.): *In Large igneous provinces: continental, oceanic and planetary flood volcanism*. Geophysical Monograph 100, 217–241. Americam Geophysical Union, Washington, DC.

Peate, D.W. & Hawkesworth, C.J., 1996: Lithospheric to asthenospheric transition in Low-Ti flood basalts from southern Paraná, Brazil. *Chemical Geology 127*, 1–24.

Riley, T.R., Leat, P.T., Curtis, M.L., Millar, I.L., Duncan, R.A. & Fazel, A., 2005: Early-middle Jurassic dolerite dykes from Western Dronning Maud Land (Antarctica): identifying mantle sources in the Karoo large igneous province. *Journal of Petrology 46*, 1489–1524.

Rudnick, R.L., & Gao, S., 2003: The composition of the continental crust. *In* R.L. Rudnick (ed.): *The crust: treatise on geochemistry* (H.D. Holland & K.K. Turekian (eds.)), 1–64. v.3. Elsevier-Pergamon, Oxford.

Scherbak, N.P., Artemenko, G.V., Lesnaya, I.M., Ponomarenko, O.M. & Shumlyanskyy, L.V., 2008: *Geokhronologiya rannego dokembriya. Proterozoj*

[Geochronology of the Early Precambrian. Proterozoic]. Naukova Dumka Publisher, Kyiv. 240 pp [In Russian].

Scherbakov, I.B., 2005: *Petrologiya Ukrainskogo schita* [Petrology of the Ukrainian Shield]. ZUKC, Lviv. 366 pp [In Russian].

Shestopalova, E.E., Stepanyuk, L.M., Dovbush, T.I., Semka, V.O., Bondarenko, S.M. & Prykhodko, E.S., 2013: Paleoproterozojskij granitoidnyj magmatism Ingulskogo megabloka Ukrainskogo schita [Palaeoproterozoic granitoid magmatism of the Ingul terrain of the Ukrainian shield]. *In Granitoids: Conditions of their Formation and Ore Potential. Proceedings of the Scientific Conference*, 152–154. M.P. Semenenko Institute of Geochemistry, Mineralogy and Ore Formation, Kyiv [In Russian].

Shumlyanskyy, L.V., 2008: Petrologiya dolerytiv Tomashgorodskoj grupy dajok (Ukrajinsky schyt) [Petrology of dolerites of the Tomashgorod dyke swarm, the Ukrainian shield]. *Mineralogichny Zhurnal 30* (2), 17–35 [In Ukrainian].

Shumlyanskyy, L.V., 2012: Evolutsiya vendskogo trapovogo magmatyzmu Volyni [Evolution of the Vendian flood basalt magmatism of the Volyn area]. *Mineralogichny Zhurnal 34* (4), 50–68 [In Ukrainian].

Shumlyanskyy, L.V., Andréasson, P.-G., Buchan, K.L. & Ernst, R.E., 2007: The Volynian Flood Basalt Province and coeval (Ediacaran) magmatism in Baltoscandia and Laurentia. *Mineralogichny Zhurnal 29* (4), 47–55.

Shumlyanskyy, L., Billström, K., Hawkesworth, C. & Elming, S.-A., 2012: U–Pb age and Hf isotope compositions of zircons from the north-western region of the Ukrainian shield: mantle melting in response to post-collision extension. *Terra Nova 24*, 373–379.

Shumlyanskyy, L., Tsymbal, S., Billström, K. & Bogdanova, S., 2010: Isotope systematics of the Ukrainian shield kimberlites. *In Abstract Volume of the Conference "Alkaline Rocks: Petrology, Mineralogy, Geochemistry"*, Kyiv, Ukraine, 19–21 September, 2010.

Smithies, R.H., Van Kranendonk, M.J. & Champion, D.C., 2005: It started with a plume – early Archaean basaltic proto-continental crust. *Earth and Planetary Science Letters 238*, 284–297.

Stepanyuk, L.M., Andrienko, O.M., Dovbush, T.I. & Bondarenko, V.K., 2005: Vik formuvannya porid Novoukrajinskogo masyvu [The age of formation of rocks of the Novoukrainka massif]. *Mineralogichny Zhurnal 27* (1), 44–50 [In Ukrainian].

Stepanyuk, L.M., Dovbush, T.I., Bondarenko, S.M., Syomka, V.O., Grinchenko, O.V. & Skurativsky, S.E., 2012: U-Pb geokhronologiya porid K-U formatsyi Ingulskogo megabloku Ukrajinskogo schyta [U-Pb geochronology of rocks of the K-U formation of the Ingul terrain of the Ukrainian shield]. *Mineralogichny Zhurnal 34* (3), 55–63 [In Ukrainian].

Stacey, J.S. & Kramers, J.D., 1975: Approximation of terrestrial lead isotope evolution by a two-stage model. *Earth and Planetary Science Letters 26*, 207–221.

Taylor, S.R. & McLennan, S.M., 1985: *The continental crust: its composition and evolution*. Blackwell, Oxford.

Tsymbal, S.N., 2013: Kimberlites of the Kirovograd ore district. *In* V.I. Starostenko, & O.B. Gintov (eds.): *Kimberlity Kirovogradskogo rudnogo rajona* [Kimberlites of the Kirovograd ore district], 390–440. Prastye Ludy Publisher, Kyiv [In Russian].

Tsymbal, S.N. & Kryvdik, S.G., 1999: Ksenolity glubinnyh porod iz kimberlitov Kirovogradskogo geobloka (Ukrainskij schit) [Xenoliths of deep-seated rocks from kimberlites of the Kirovograd area, Ukrainian shield]. *Mineralogichny Zhurnal 21* (2/3), 97–111 [In Russian].

Tsymbal, S.N., Kryvdik, S.G., Kiryanov, N.N. & Makivchuk, O.F., 1999: Sostav kimberlitov Kirovogradskogo bloka [Composition of the Kirovograd area kimberlites, Ukrainian shield]. *Ukrainskij Schit. Mineralogichny Zhurnal 21* (2/3), 22–38 [In Russian].

Tsymbal, S.N., Kryvdik, S.G., Shumlyanskyy, L.V., Bogdanova, S.V. & Tsymbal, Yu. S., 2011: Sostav i vozrast subschelochnykh gabbroidov dajkovogo kompleksa tsentralnoj chasti Kirovogradskogo megabloka Ukrainskogo schita [Composition and age of subalkaline gabbroic dykes of the central part of the Kirovograd terrain of the Ukrainian shield]. *In Ore potential of the alkaline, kimberlitic and carbonatitic magmatism: Proceedings of the XXVIII International Conference* (Minsk, 9–16 September 2011), 190–192 [In Russian].

Usenko, I.S., Scherbakov, I.B. & Siroshtan, R.I., 1982: *Metamorfizm Ukrainskogo schita* [The metamorphism of the Ukrainian shield]. Naukova Dumka Publisher, Kyiv. 308 pp [In Russian].

Weaver, B.L., 1991: The origin of ocean island basalt end-member compositions: trace element and isotopic constraints. *Earth and Planetary Science Letters 104*, 381–397.

Yutkina, E.V., Kononova, V.A., Tsymbal, S.N., Levskiy, L.K. & Kiryanov, N.N., 2005: Izotopno-geokhimicheskaya spetsializatsiya mantijnogo istochnika kimberlitov Kirovogradskogo kompleksa (Ukrainskij schit) [Isotope-geochemical specialisation of the mantle source of kimberlites of the Kirovograd complex, Ukrainian Shield]. *Doklady Akademii Nauk 402*, 87–91 [In Russian].

Zankevych, B.O., Mykhalchenko, I.I., Ponomarenko, O.M., 2014: Geodynamichni peredumovy U mineralizatsyij v Ingulskomu megablotsi Ukrajinskogo schyta. *In Geochronology and geodynamics of the early precambrian (3.6–1.6 Ga) of the Eurasian Continent. Abstract Volume of the International Conference Dedicated to the 90th Anniversary of Academician Scherbak M.P. Kyiv* [Geological-dynamic preconditions of U mineralization in the Ingul area of the Ukrainian shield], 16–17 September 2014, 48–49 [In Ukrainian].